nature geoscience

Article

https://doi.org/10.1038/s41561-025-01889-9

Deglaciation of the Prudhoe Dome in northwestern Greenland in response to Holocene warming

Received: 28 February 2025

Accepted: 24 November 2025

Published online: 05 January 2026

Check for updates

Caleb K. Walcott-George[1,2] ✉, Nathan D. Brown[3], Jason P. Briner[1], Allie Balter-Kennedy[4,5], Nicolás E. Young[4], Tanner Kuhl[6], Elliot Moravec[6], Sridhar Anandakrishnan[7], Nathan T. Stevens[8], Benjamin Keisling[9], Robert M. DeConto[10], Vasileios Gkinis[11], Joseph A. MacGregor[12] & Joerg M. Schaefer[4]

Projections of future sea-level rise benefit from understanding the response of past ice sheets to warming during past Quaternary interglacials. Constraints on the extent of inland Greenland Ice Sheet retreat during the Middle Holocene (~8–4 thousand years before present) are limited because geological records of a smaller-than-modern phase largely remain beneath the modern ice sheet. We drilled through 509 metres of firn and ice at Prudhoe Dome, northwestern Greenland, to obtain sub-ice material yielding direct evidence for the response of the northwest Greenland ice sheet to Holocene warmth. Here we present infrared stimulated luminescence measurements from sub-ice sediments that indicate that the ground below the summit was exposed to sunlight 7.1 ± 1.1 thousand years ago. This proposed complete deglaciation of Prudhoe Dome, coeval to reduced extent at other ice caps across northern Greenland, is consistent with interglacial-only $\delta^{18}O$ values from the Prudhoe Dome ice column and ice depth–age modelling. Our results point to a substantial response of the northwest Greenland ice sheet to early Holocene warming, estimated to be +3–5 °C from palaeoclimate data. This range of summer temperatures is similar to projections of warming by 2100 CE.

The Greenland Ice Sheet (GrIS) has waxed and waned over the Quaternary, nearly completely deglaciating at least once in the last 1.1 Myr (ref. 1). Evaluating the response of the GrIS to past warming is necessary to predict the future response of the ice sheet and its contributions to sea-level rise[2]. Existing reconstructions using lake sediment records and radiocarbon dating of reworked organic materials found in Little Ice Age deposits suggest the central and southern GrIS retreated to its minimum Holocene size between ~5 and ~3 thousands of years before present (ka) before readvancing to its historical maximum (nomenclature on Greenland for the recent ice extent that often occurred during the Little Ice Age[3]) at ~1850 CE and provide an important framework for evaluating GrIS response to the most recent warm period[4]. However, these studies usually provide loose constraints on the ice sheet footprint during these minima, making it difficult to assess the specific local responses of the GrIS to Holocene warmth. Meanwhile, cosmogenic nuclide and luminescence dating of sub-ice materials retrieved from ice core drilling campaigns can provide direct constraints on when locations in Greenland's far interior were ice free in the past, resulting in more precise depictions of ice sheet geometry[1,5]. These studies have spurred new drilling projects aiming to assess the magnitude of GrIS inland retreat during the Holocene and its reaction to Holocene warmth by collecting sub-ice sediments and bedrock from key locations around the margins of the GrIS that can provide constraints on past ice sheet extents[6,7]. We present new infrared stimulated luminescence (IRSL)

A full list of affiliations appears at the end of the paper. ✉e-mail: c.wg@uky.edu

https://doi.org/10.1038/s41561-025-01889-9

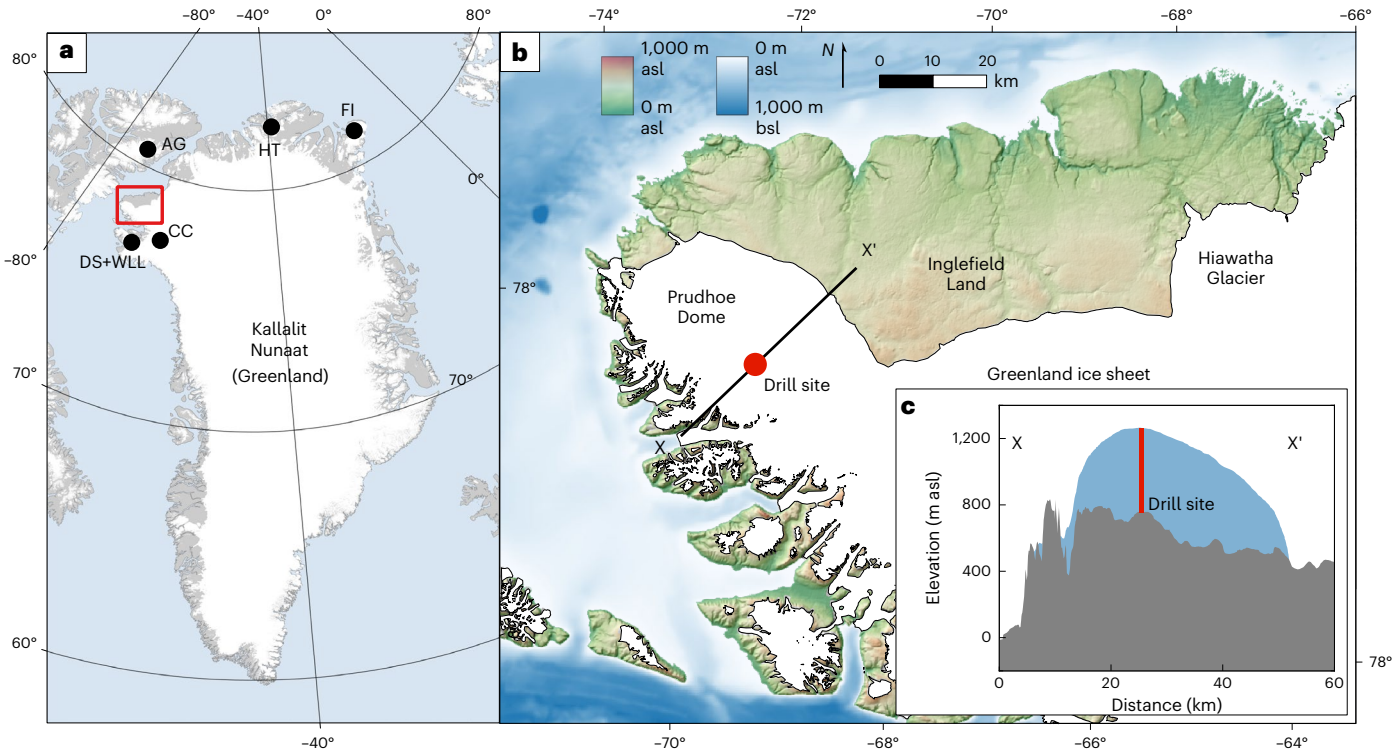

Fig. 1 | Maps of study area. a, Map of Greenland and surrounding areas with modern ice extents[37] showing study site in red box and the locations of Hans Tausen (HT) and Flade Isblink (FI) ice caps, the Camp Century ice core site (CC), the Agassiz Ice Cap ice core site (AG) and Deltasø (DS) and Wax Lips (WLL) lakes. **b**, Digital elevation map[38] of areas surrounding Prudhoe Dome showing drill site. m asl, meters above sea level; m bsl, meters below sea level. **c**, Cross section shows ice thickness and bedrock topography of Prudhoe Dome measured by radar sounding[39] and the drill site.

measurements from sub-ice sediments below the summit of Prudhoe Dome (PD), $\delta^{18}O$ (the deviation in the ratio of oxygen-18 relative to a known standard) measurements of the overlying ice column and simple one-dimensional (1-D) ice depth–age modelling to provide robust evidence that PD deglaciated during the Holocene.

Prudhoe Dome, northwestern Greenland, is an ~2,500 km^2 ice dome with a maximum ice thickness of ~600 m attached to the main body of the GrIS via a saddle (Fig. 1). To its north and east, PD terminates at Inglefield Land, whereas its western and southern portions mostly terminate as marine outlet glaciers between narrow highlands. A recent synthesis of simulated GrIS basal thermal state indicates that the bed of PD is probably cold based[8]. Intensely weathered bedrock surfaces with high concentrations of cosmogenic nuclides suggest that the GrIS was mostly cold based when it covered Inglefield Land during the Quaternary[9,10]. During the Last Glacial Maximum (LGM; 26–19 ka), this sector of the GrIS expanded into Nares Strait, where it merged with the Innuitian Ice Sheet and flowed southward into northern Baffin Bay[11,12]. Ice retreated to the coast of modern-day Inglefield Land by ~9 ka, before reaching the present GrIS margin in central Inglefield Land at ~7 ka (refs. 13–16). After ~7 ka, the GrIS continued to retreat to a smaller-than-modern position until it began readvancing to its Little Ice Age maximum[16]. The extent of the inland retreat of PD during the Holocene, and the timing of minimum extent, remains unknown. To assess this, we collected 3.0 m of sediment above 4.4 m of bedrock from a topographic high under 509.4 m of ice at the centre of PD. We also retained ice chips from the ice column for $\delta^{18}O$ measurements, which provide information on the presence or absence of Pleistocene ice at the site.

The Holocene deglaciation of PD

Luminescence ages from sediments record the duration since sediment grains were last exposed to sunlight. Minimum dose models of single-grain equivalent dose (D_e) derived from IRSL measurements on sand-sized K-feldspar from a massive sand and angular gravel diamict (Extended Data Figs. 1 and 2) in the upper 7.5 cm of the sub-ice sediments yield a burial age of 7.1 ± 1.1 ka (Methods). Our depth profile of D_e estimates reveals a sharp decrease of D_e towards the uppermost sediments; values at depth (~180 cm) of ~100 Gray (Gy) decrease to 14.4 ± 2.2 Gy at 0–2.5 cm (Fig. 2b).

At our site under the centre of PD, exposure of sediment grains to sunlight occurs when PD is absent. Therefore, the burial age of our uppermost sediments of 7.1 ± 1.1 ka unambiguously requires PD to have deglaciated from our ice dome summit drill site during the Holocene. Decreasing D_e values towards the surface are consistent with sediment mixing in the upper ~10 cm (refs. 17,18). During sediment mixing, fully bleached grains from the surface become mixed deeper into the sediment column and deeper grains are brought closer to the surface, where some become fully bleached (Fig. 3). Given the high Arctic setting of our site, we suggest that during this period of Holocene ice-free conditions, sediment mixing was driven by cryoturbation of an active layer within continuous permafrost sediments—a dominant driver of soil reworking in Arctic environments[19]. The presence of continuous, massive diamict from the surface to ~47 cm also supports our hypothesis of in situ mixing, as we find no evidence that the uppermost sediments are sedimentologically different (Extended Data Figs. 1 and 2). Such mixing would occur until ice cap formation at the ice divide (the location of our drill site) as snow accumulated and compressed into ice, causing cryoturbation to cease as the sediments became perennially frozen. Meanwhile, the previously bleached sediments would begin to record this burial duration. Additionally, because our drill site is at the centre of PD along the ice divide (where there is zero horizontal velocity), we posit that the sediments within our core remained in situ during ice cap regrowth, rather than being transported from elsewhere.

https://doi.org/10.1038/s41561-025-01889-9

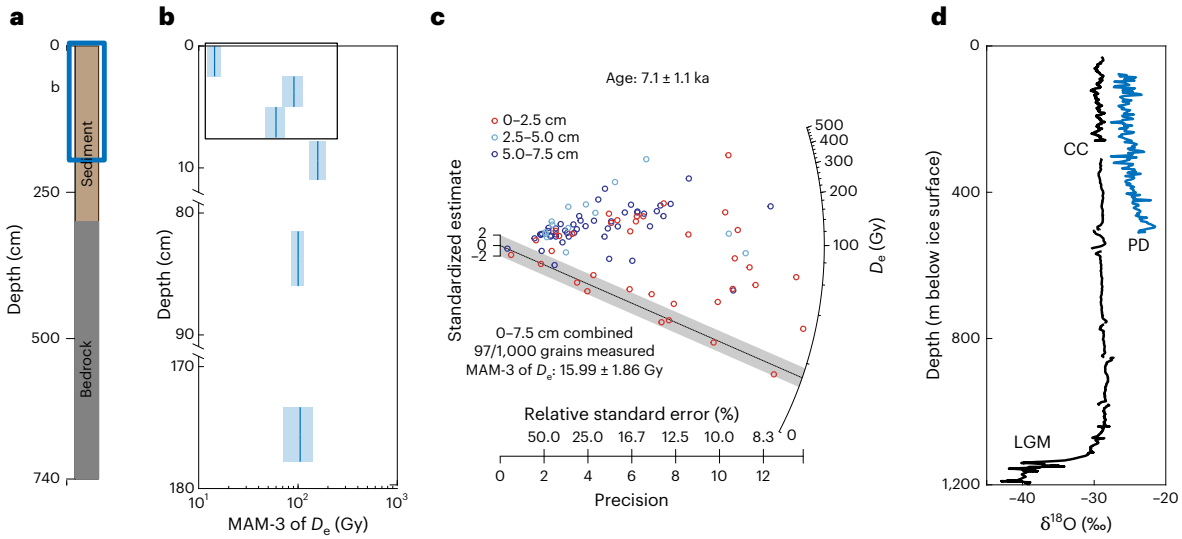

Fig. 2 | Luminescence and δ^{18}O measurements. a, Simplified stratigraphic log of the ASIG (Agile Sub-Ice Geological Drill) core; blue box shows location of IRSL measurements in panel **b**. **b**, Minimum dose model (MAM-3) of single-grain D_e with depth. Blue line represents mean and transparent blue box represents the 1σ error. Black box shows upper 0–7.5 cm used to calculate burial age in panel. Breaks in *y*-axis are included to cover only the sediment sections where we made luminescence measurements. **c**, Radial plot of single-grain K-feldspar measurements combined for grains (each grain measurement is an open circle) from 0 to 7.5 cm, and depths of individual grains are noted by varying colours. Grey dashed line shows MAM-3 estimates of D_e 2σ error (grey bar). Supplementary Fig. 1 provides additional details on interpreting luminescence radial plots. Grains within the grey bar are represented by the pink grains in Fig. 3d, whereas grains outside the grey bar are represented by the red grains in Fig. 3d. **d**, δ^{18}O measurements from the overlying ice at our drill site (PD) measured every ~ 3 m, along with measurements from the Camp Century (CC) ice core[40].

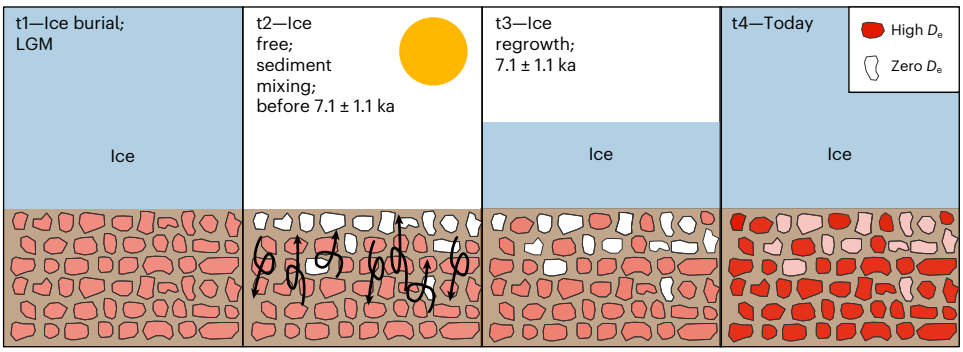

Fig. 3 | Conceptual model of luminescence resetting through sediment mixing during ice-free periods. t1, Sediments are buried beneath ice and each individual grain is accumulating a luminescence signal (light red). t2, Ice retreats, exposing the uppermost sediments to sunlight, resetting the luminescence signal (white grains). Sediment is mixed, bringing some grains with no luminescence signal (white) lower in the column and some grains with pre-existing luminescence signals towards the surface (light red). t3, Ice regrows over the sediment, cutting off sunlight. Sediments that saw sunlight before burial have no luminescence signal (white), whereas sediments that were not brought to the surface retain luminescence signals (light red); sediment mixing has pooled together these grains with differing luminescence signals, where a minimum age model can identify the youngest population of grains (Fig. 2c). t4, Sediment grains that saw sunlight during t2 (pink) record burial ages since ice regrowth (dots in grey bar in Fig. 2c). Sediment grains that did not see sunlight during t2 (dark red) have luminescence that built up during multiple periods of ice burial (grains outside of grey bar in Fig. 2d).

The skewed distribution of our D_e values with a population of low D_e grains among a larger population of higher D_e grains supports this hypothesis, as only a portion of grains became bleached during Holocene deglaciation (Figs. 2b and 3). We interpret our IRSL age from the upper 7.5 cm of sediment (7.1 ± 1.1 ka) as recording the cessation of sediment mixing and the initiation of PD regrowth, thus serving as a minimum age for deglaciation and a maximum age for reglaciation. Additionally, we observe no major decrease in δ^{18}O in PD ice, similar to that seen in the Camp Century ice core record at ~1,050 m, representing Pleistocene ice (Fig. 2d). An apparent lack of Pleistocene ice in the PD ice column requires that PD fully melted following the Younger Dryas and then reformed during the Holocene. This finding is also compatible with the majority (14 of 25 model instances) of plausible 1-D ice age–depth models of the ice column that predict only Holocene ice ages there, with basal ice that dates to before ~5 ka (Extended Data Fig. 3).

The glacial history of northern Greenland

The deglaciation of PD during the Holocene is compatible with other records of ice cap recession across northern Greenland (Fig. 4). A proglacial lake sediment record from Deltasø reveals that the North Ice Cap, ~180 km south of Prudhoe Dome, was smaller than present or absent from ~10.1 ka to 1850 CE (ref. 20). An age–depth model based on evidence of known-age volcanic eruptions recorded in a 345-m-long ice core from Hans Tausen Ice Cap in northern Greenland (Fig. 1) suggest it completely deglaciated sometime during the Holocene and later regrew between 4.0 and 3.5 ka (ref. 21). Proglacial threshold lake records show that Flade Isblink ice cap (Fig. 1) was smaller than present from

https://doi.org/10.1038/s41561-025-01889-9

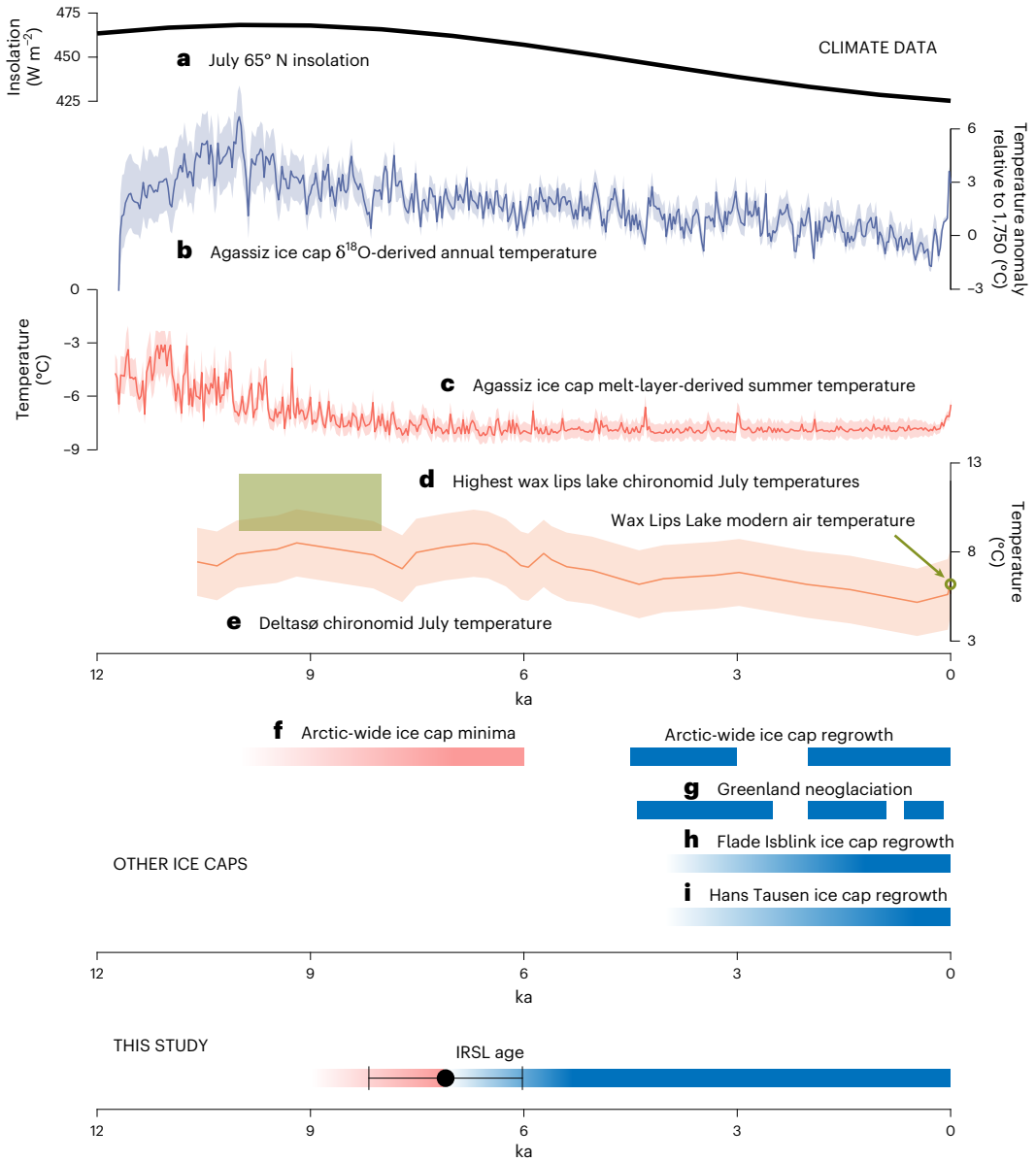

Fig. 4 | Regional palaeoclimate data compared against records of Arctic ice cap retreat and growth. a–**d**, Regional palaeoclimate data (Fig. 1) compared against records of Arctic ice cap retreat/absence (red) and growth/presence (blue). **a**, July insolation at 65° (ref. 41). **b**, Agassiz Ice Cap annual $\delta^{18}O$ temperature record with 2σ error[31]. **c**, Agassiz Ice Cap summer melt-layer temperature record with 2σ error[31]. **d**, Wax Lips Lake, NW Greenland, chironomid July temperature estimates and modern temperature[32]. **e**, Deltasø, NW Greenland, chironomid July temperature reconstructions with 1σ error[23]. **f**, Summarized records of Arctic ice cap minima and re-growth[27]. **g**, Summary of Greenland Ice Sheet Neoglaciation[31]. **h**, Flade Isblink ice cap regrowth[26]. **i**, Hans Tausen ice cap regrowth[24]. Black dot (mean) and 1σ error bars show IRSL burial age of the uppermost 7.5 cm from our sub-ice sediment core, derived from luminescence measurements on 1,000 individual K-feldspar grains (Methods). Red bar shows period of PD deglaciation from modern coast of Inglefield Land[12–15] and blue shows regrowth/presence after deglaciation.

~9.4 to 0.2 ka and that at least parts of the ice cap may have persisted throughout the Holocene[22]. Ice-flow modelling and stable isotope measurements from an ice core suggest the main portion of Flade Isblink ice cap formed after 4.0 ka (ref. 23). Across much of the Arctic, ice caps began to regrow by ~4 ka following their Holocene minima (Fig. 4)[24,25].

Reviews of existing GrIS margin chronologies suggest that ice retreat behind the modern margin was spatially heterogeneous across Greenland, though it probably reached its minimum extent during the Middle/Late Holocene (~ 5–3 ka) and experienced several pronounced periods of Neoglaciation[4,26–28]. However, its exact geometry is unknown and there is likely substantial variability in the timing of that minimum extent across Greenland. In Inglefield Land, Hiawatha Glacier was smaller than today from > 5.8 to < 1.9 ka, whereas Humboldt Glacier retreated behind its present margin from sometime between > 3.6 and < 0.5 ka (ref. 16). These records of ice cap and GrIS retreat suggest a complex pattern of ice sheet response to Holocene climate fluctuations.

Drivers of northern Greenland deglaciation and regrowth

The deglaciation of PD broadly aligns with higher-than-modern Holocene temperatures reconstructed across other parts of Greenland between 10 and 4 ka, with large spatial variability[4,28]. Much of PD is land terminating today and was probably completely land terminating during Holocene deglaciation, as it retreated within its modern footprint and out of the fjords on its southern flanks. Thus retreat and ultimately complete deglaciation would not have been influenced by

ice–ocean interactions such as calving and submarine melting but mostly governed by summer melt (surface mass balance). Summer temperatures reached their maximum in northwestern Greenland between ~10 and ~7 ka, as recorded by chironomid assemblages in lake sediment cores indicating July temperatures ~3 to 7 °C warmer than modern[20,25,29]. Similarly, a melt-layer-derived summer temperature record from nearby Agassiz Ice Cap on Ellesmere Island reveal temperatures ~3 °C higher than modern between ~11 and 9 ka (ref. 30). Meanwhile a coeval $\delta^{18}O$-based record of mean annual temperatures from Agassiz Ice Cap shows ~3–6 °C of warming in the Early/Middle Holocene[30]. It appears that substantial Early and Middle Holocene atmospheric warming drove increased surface melting to the point of completely melting PD.

The full melt and regrowth of PD during the Early–Middle Holocene points to an early and high amplitude summer warm anomaly in northwestern Greenland, as evidenced in palaeoclimate records[24,25,31]. While a recent ice core synthesis indicates a near-uniform Holocene Thermal Maximum (HTM) onset by the mid-Holocene, our record from PD suggests an earlier summer HTM, with Holocene summer temperatures high enough to melt PD before 7.1 ± 1.1 ka (ref. 32). Summer temperatures then had to decrease sufficiently to subsequently regrow PD within a few millennia. The Agassiz Ice Cap melt-layer-derived summer temperature record shows cooling in the early Holocene, but this proxy does not quantify temperatures below −8 °C and thus does not record any potential cooling below this threshold[30]. Proxy data from nearby lakes suggest elevated summer temperature was declining by ~8 ka (ref. 29). Combined, available data suggest an early termination to summer HTM conditions paired with relatively steady precipitation through the Holocene[33]. However, given the differences in seasonality recorded in ice core records and the ablation-driven retreat of PD, an increase in winter temperatures may partially obfuscate some summer cooling, leading to a temporal mismatch between summer and annual HTM conditions, making it difficult to assess the climate conditions leading to the regrowth of PD[25,32]. We suspect that even subtle climate shifts following the HTM, in which the snowline descended to intersect the elevated topography below the PD summit, could be sufficient to regrow PD to its modern configuration via self-amplifying elevation feedbacks. Such large summer Holocene temperature changes in northwestern Greenland may implicate Arctic amplification (for example, sea–ice feedbacks) in leading to higher amplitude Holocene summer temperature change in northern versus southern Greenland[4,25,34].

The magnitude of increased summer temperatures at the time of PD deglaciation are within the range of simulated 2100 CE summer warming at PD of between 1.8 and 4.7 °C (CMIP5 (Coupled Model Intercomparison Project)) and 2.4 and 5.7 °C (CMIP6)[35]. Given the likelihood that CMIP projections underestimate the magnitude and rate of Arctic amplification (and therefore warming), summer temperatures at PD will probably reach levels that led to its Holocene deglaciation by 2100[36]. However, the duration required to deglaciate PD under these elevated temperatures remain unconstrained, suggesting that mitigation of future warming might ameliorate future melting of PD.

Luminescence analysis of sub-ice materials constrain the timing of minimum ice extent within the current GrIS footprint. Our IRSL age paired with $\delta^{18}O$ measurements and ice accumulation modelling unambiguously indicate the deglaciation and subsequent reglaciation of Prudhoe Dome during the Early–Middle Holocene, pointing to a highly sensitive northern GrIS. This motivates future drilling efforts across the GrIS and peripheral ice caps to map the spatial pattern of inland retreat during the Holocene, offering additional insights into the evolution of the GrIS under elevated Arctic warming.

Online content

Any methods, additional references, Nature Portfolio reporting summaries, source data, extended data, supplementary information, acknowledgements, peer review information; details of author contributions and competing interests; and statements of data and code availability are available at https://doi.org/10.1038/s41561-025-01889-9.

References

1. Schaefer, J. M. et al. Greenland was nearly ice-free for extended periods during the Pleistocene. *Nature* **540**, 252–255 (2016).
2. Briner, J. P. et al. Rate of mass loss from the Greenland Ice Sheet will exceed Holocene values this century. *Nature* **586**, 70–74 (2020).
3. Weidick, A., Bennike, O., Citterio, M. & Nørgaard-Pedersen, N. Neoglacial and historical glacier changes around Kangersuneq fjord in southern West Greenland. *GEUS Bull.* **27**, 1–68 (2012).
4. Briner, J. P. et al. Holocene climate change in Arctic Canada and Greenland. *Quat. Sci. Rev.* **147**, 340–364 (2016).
5. Christ, A. J. et al. Deglaciation of northwestern Greenland during Marine Isotope Stage 11. *Science* **381**, 330–335 (2023).
6. Briner, J. P. et al. Drill-site selection for cosmogenic-nuclide exposure dating of the bed of the Greenland Ice Sheet. *Cryosphere* **16**, 3933–3948 (2022).
7. Keisling, B. A. et al. An ice-sheet modelling framework for leveraging sub-ice drilling to assess sea level potential applied to Greenland. *EGUsphere* **2024**, 1–25 (2024).
8. MacGregor, J. A. et al. GBaTSv2: a revised synthesis of the likely basal thermal state of the Greenland Ice Sheet. *Cryosphere* **16**, 3033–3049 (2022).
9. Walcott-George, C. K., Balter-Kennedy, A., Briner, J. P., Schaefer, J. M. & Young, N. E. Glacial erosion and history of Inglefield Land, northwestern Greenland. *Cryosphere* **19**, 2067–2086 (2025).
10. Søndergaard, A. S. et al. Multi-million-year evolution of the Greenland Ice Sheet in Inglefield Land, North Greenland. *J. Quat. Sci.* **40**, 1056–1069 (2025).
11. Leger, T. P. M. et al. A Greenland-wide empirical reconstruction of paleo ice sheet retreat informed by ice extent markers: paleoGrIS version 1.0. *Clim* **20**, 701–755 (2024).
12. Batchelor, C. L., Krawczyk, D. W., O'Brien, E. & Mulder, J. Shelf-break glaciation and an extensive ice shelf beyond northwest Greenland at the Last Glacial Maximum. *Mar. Geol.* **476**, 107375 (2024).
13. Mason, O. K. Beach ridge geomorphology at Cape Grinnell, northern Greenland: a less icy Arctic in the mid-Holocene. *Geogr. Tidsskr.-Dan. J. Geogr.* **110**, 337–355 (2010).
14. Nichols, R. L. Geomorphology of Inglefield land, north Greenland. *Medd. Grønl.* **188**, 3–105 (1969).
15. Blake, W., Boucherle, M. M., Fredskild, B., Janssens, J. A. & Smol, J. P. The geomorphological setting, glacial history and Holocene development of Kap Inglefield Sø, Inglefield Land, North-West Greenland. *Medd. Grønl.: Geosci.* **27**, 1–42 (1992).
16. Søndergaard, A. S. et al. Glacial history of Inglefield Land, north Greenland from combined in situ ^{10}Be and ^{14}C exposure dating. *Climate* **16**, 1999–2015 (2020).
17. Gray, H. J., Keen-Zebert, A., Furbish, D. J., Tucker, G. E. & Mahan, S. A. Depth-dependent soil mixing persists across climate zones. *Proc. Natl Acad. Sci. USA* **117**, 8750–8756 (2020).
18. Reimann, T., Román-Sánchez, A., Vanwalleghem, T. & Wallinga, J. Getting a grip on soil reworking–single-grain feldspar luminescence as a novel tool to quantify soil reworking rates. *Quat. Geochronol.* **42**, 1–14 (2017).
19. Bryan, K. Cryopedology, the study of frozen ground and intensive frost-action, with suggestions on nomenclature. *Am. J. Sci.* **244**, 622–642 (1946).
20. Axford, Y. et al. Holocene temperature history of northwest Greenland—with new ice cap constraints and chironomid assemblages from Deltasø. *Quat. Sci. Rev.* **215**, 160–172 (2019).

21. Clausen, H. B. et al. Glaciological and chemical studies on ice cores from Hans Tausen Iskappe, Greenland. *Medd. Grønl.: Geosci.* **39**, 123–149 (2001).
22. Larsen, N. K. et al. Local ice caps in Finderup land, north Greenland, survived the Holocene thermal maximum. *Boreas* **48**, 551–562 (2019).
23. Lemark, A. & Dahl-Jensen, D. *A Study of the Flade Isblink Ice Cap Using a Simple Ice Flow Model*. MSc thesis, Niels Bohr Institute, Copenhagen Univ. (2010).
24. Larocca, L. J. & Axford, Y. Arctic glaciers and ice caps through the Holocene: a circumpolar synthesis of lake-based reconstructions. *Clim* **18**, 579–606 (2022).
25. Axford, Y., De Vernal, A. & Osterberg, E. C. Past warmth and its impacts during the Holocene thermal maximum in Greenland. *Annu. Rev. Earth Planet. Sci.* **49**, 279–307 (2021).
26. Young, N. E. & Briner, J. P. Holocene evolution of the western Greenland Ice Sheet: assessing geophysical ice-sheet models with geological reconstructions of ice-margin change. *Quat. Sci. Rev.* **114**, 1–17 (2015).
27. Larsen, N. K. et al. The response of the southern Greenland ice sheet to the Holocene thermal maximum. *Geology* **43**, 291–294 (2015).
28. Kjær, K. H. et al. Glacier response to the Little Ice Age during the Neoglacial cooling in Greenland. *Earth Sci. Rev.* **227**, 103984 (2022).
29. McFarlin, J. M. et al. Pronounced summer warming in northwest Greenland during the Holocene and Last Interglacial. *Proc. Natl Acad. Sci. USA* **115**, 6357–6362 (2018).
30. Lecavalier, B. S. et al. High Arctic Holocene temperature record from the Agassiz ice cap and Greenland ice sheet evolution. *Proc. Natl Acad. Sci. USA* **114**, 5952–5957 (2017).
31. Renssen, H., Seppä, H., Crosta, X., Goosse, H. & Roche, D. M. Global characterization of the Holocene Thermal Maximum. *Quat. Sci. Rev.* **48**, 7–19 (2012).
32. Martin, K. C. et al. Greenland Ice cores reveal a south-to-north difference in Holocene thermal maximum timings. *Geophys. Res. Lett.* **51**, e2024GL111405 (2024).
33. Badgeley, J. A., Steig, E. J., Hakim, G. J. & Fudge, T. J. Greenland temperature and precipitation over the last 20 000 years using data assimilation. *Clim* **16**, 1325–1346 (2020).
34. Miller, G. H. et al. Arctic amplification: can the past constrain the future?. *Quat. Sci. Rev.* **29**, 1779–1790 (2010).
35. IPCC. *Climate Change 2021: The Physical Science Basis* (eds Masson-Delmotte, V. et al.) (Cambridge Univ. Press, 2021).
36. Rantanen, M. et al. The Arctic has warmed nearly four times faster than the globe since 1979. *Commun. Earth Environ.* **3**, 168 (2022).
37. Moon, T., Fisher, M., Stafford, T. & Harden, L. QGreenland. *Zenodo* https://doi.org/10.5281/zenodo.12823307 (2023).
38. Porter, C. et al. ArcticDEM–Mosaics. *Harvard Dataverse* https://doi.org/10.7910/DVN/3VDC4W (2023).
39. Paden, J., Li, J., Leuschen, C., Rodriguez-Morales, F. & Hale, R. IceBridge accumulation radar L1B geolocated radar echo strength profiles, version 2. *NASA National Snow and Ice Data Center Distributed Active Archive Center* https://doi.org/10.5067/0ZY1XYHNIQNY (2014).
40. Johnsen, S. J., Dansgaard, W., Clausen, H. B. & Langway, C. C. Oxygen isotope profiles through the Antarctic and Greenland ice sheets. *Nature* **235**, 429–434 (1972).
41. Berger, A. & Loutre, M.-F. Insolation values for the climate of the last 10 million years. *Quat. Sci. Rev.* **10**, 297–317 (1991).

[1]Department of Earth Sciences, University at Buffalo, Buffalo, NY, USA. [2]Department of Earth and Environmental Sciences, University of Kentucky, Lexington, KY, USA. [3]Department of Earth and Environmental Sciences, University of Texas at Arlington, Arlington, TX, USA. [4]Lamont-Doherty Earth Observatory, Columbia University, Palisades, NY, USA. [5]Department of Earth and Climate Sciences, Tufts University, Medford, MA, USA. [6]NSF Ice Drilling Program, University of Wisconsin, Madison, WI, USA. [7]Department of Geosciences, Pennsylvania State University, University Park, PA, USA. [8]Pacific Northwest Seismic Network, University of Washington, Seattle, WA, USA. [9]Institute for Geophysics, University of Texas at Austin, Austin, TX, USA. [10]Department of Geoscience, University of Massachusetts, Amherst, MA, USA. [11]Physics of Ice, Climate and Earth, Niels Bohr Institute, University of Copenhagen, Copenhagen, Denmark. [12]Cryospheric Sciences Laboratory, NASA Goddard Space Flight Center, Greenbelt, MD, USA. ✉e-mail: c.wg@uky.edu

Methods

Sub-ice drilling, ice, sediment and bedrock collection

We used the Agile Sub-Ice Geologic (ASIG) drill operated by the NSF (National Science Foundation) Ice Drilling Program to drill through PD and access the ice sheet bed at a geophysically constrained topographic high (880 m above sea level (asl)) at the ice divide (1,390 m asl). We collected ice chips from drill cuttings every ~3 m for $\delta^{18}O$ measurements of the ice column. At 509.4 m ice depth, the drill encountered the ice sheet bed upon which return fluid included sand grains along with the ice chips. We then collected a 7.5-m-long core, comprising 3 m of frozen sediment on top of 4.5 m of gneissic bedrock. The upper 7.5 cm of the sediment core, drilled immediately after flushing the sediment-bearing cuttings, were kept in lightproof conditions for luminescence dating.

Luminescence dating

We sub-divided the light-shielded upper 7.5 cm into three segments at 2.5-cm intervals. We later sub-sampled inner portions of the core at 8.0–11.2 cm, 81.5–88.0 cm and 167.9–173.2 cm under amber light at −20 °C. We melted samples under amber light conditions at the University of Texas at Arlington Luminescence Lab (UTALL), where we used standard heavy liquids and acid treatment to isolate 150–200 µm potassium feldspar grains. We determined equivalent dose (D_e) values for individual K-feldspar grains from each depth interval using single-grain post-infrared infrared stimulated luminescence measured at 225 °C (p-IR $IRSL_{225}$)[42]. To test for fading, grains were irradiated, preheated and then held at room temperature for delays ranging from about 23 minutes to 2 weeks (ref. 43). No signal fading was observed on these timescales (Supplementary Fig. 8). We calculated cumulative D_e estimates for each depth interval and the combined measurements from 0–7.5 cm using a three-variable minimum age model (MAM-3) assuming 15% overdispersion for single dose populations (Supplementary Table 1)[44]. We sent aliquots (1–10 g) of material from four depth intervals, 0–7.5 cm, 8.0–11.2 cm, 81.5–88.0 cm and 173.3–177.8 cm for X-ray fluorescence (XRF) and inductively coupled plasma mass spectrometry (ICP-MS) measurements of radionuclides at SGS Canada (0–7.5 cm) or the Washington State University Peter Hooper GeoAnalytical Lab (8.0–11.2 cm, 81.5–88.0 cm and 173.3–177.8 cm). We measured water content by measuring the mass of samples before melting and again after melting and after drying sediments in a 50 °C oven overnight. We calculated environmental dose rates for each segment of 2.5 cm from the upper 7.5 cm using alpha, beta and gamma infinite matrix dose rates from the Dose Rate and Age Calculator (DRAC), assuming inert overburden ice and a depth-dependent total dose rate field within the underlying sediment (Supplementary Tables 2 and 3)[45,46]. To calculate the minimum age within the upper 7.5 cm, we used the average dose rate within this interval and the minimum dose model of all grains within this interval to calculate our burial age (Supplementary Table 4).

Oxygen isotope measurements

We collected ice chips following each drill run of 3 m, which constituted a mixture of ice chips from each run. We flushed the drill hole between each run to remove residual ice chips. We performed triple water isotope analysis ($\delta^{17}O$, $\delta^{18}O$, δD) on drill ice chips using cavity ring-down spectroscopy (Picarro L-2140i) with a high-throughput vaporizer (Picarro A0212), following the protocol described in ref. 47 modified for drill chips. To prevent spectroscopic contamination from residual drill liquid, we incorporated a melt–refreeze step in the sample preparation procedure, allowing for the effective removal of organics. The sampling procedure provided a resolution of ~3 m.

Measurements are reported in per mille (‰) relative to the Vienna Standard Mean Ocean Water and Standard Light Antarctic Precipitation (VSMOW–SLAP) international scale, defined by reference materials. We used three internal water standards with well-calibrated values against VSMOW–SLAP (Table water standards). The light and heavy standard materials ('-22' and '-40') were used to construct a calibration curve, whereas the middle standard ('NEEM') served as a reference for accuracy estimation. Measurement precision was determined to be ± 0.025‰ for $\delta^{17}O$, ± 0.021‰ for $\delta^{18}O$ and ± 0.23‰ for δD.

Ice depth–age modelling

We evaluated three one-dimensional (1-D) steady-state ice-flow models to assess plausible depth–age relationships of the ice column at our PD drill site (Extended Data Fig. 3)[48]. More sophisticated, transient and three-dimensional modelling of the age of the GrIS has recently been demonstrated, but those models are presently too coarse (both spatially and temporally) to meaningfully resolve the age structure of the modern PD[49,50]. The three models are all conventionally applied for ice sheet interiors[51], and here we calculate them using a range of plausible Holocene and LGM conditions to aid first-order interpretation of our measured $\delta^{18}O$ drill ice chip record at PD. All three models are calculated analytically. Besides the local ice thickness, their differing underlying assumptions regarding local ice dynamics lead to their dependence on either one or two model parameters, one of which is always the surface accumulation rate (Nye). The other is either the basal melt rate (Nye + basal melt) or the thickness of the basal shear layer (Dansgaard–Johnsen). For each model parameter, we considered a range of five possible values and identified one of those as the most plausible based on past modelling of the GrIS, resulting in a total of 25 model instances[51,52].

Data availability

Luminescence data are available via Zenodo at https://doi.org/10.5281/zenodo.17047558 (ref. 53) and in the Supplementary Information. Oxygen isotope data are available via PANGAEA at https://doi.org/10.1594/PANGAEA.984743 (ref. 54) and in the Supplementary Information. Model data are available via Zenodo at https://doi.org/10.5281/zenodo.17048033 (ref. 55).

Code availability

MATLAB code and data used for ice depth–age modelling are available via Zenodo at https://doi.org/10.5281/zenodo.17048033 (ref. 54).

References

42. Buylaert, J. P., Murray, A. S., Thomsen, K. J. & Jain, M. Testing the potential of an elevated temperature IRSL signal from K-feldspar. *Radiat. Meas.* **44**, 560–565 (2009).
43. Galbraith, R. F., Roberts, R. G., Laslett, G. M., Yoshida, H. & Olley, J. M. Optical dating of single and multiple grains of quartz from Jinmium rock shelter, northern Australia: part I, experimental design and statistical models. *Archaeometry* **41**, 339–364 (1999).
44. Auclair, M., Lamothe, M. & Huot, S. Measurement of anomalous fading for feldspar IRSL using SAR. *Radiat. Meas.* **37**, 487–492 (2003).
45. Durcan, J. A., King, G. E. & Duller, G. A. T. DRAC: dose rate and age calculator for trapped charge dating. *Quat. Geochronol.* **28**, 54–61 (2015).
46. Sohbati, R., Murray, A. S., Porat, N., Jain, M. & Avner, U. Age of a prehistoric 'Rodedian' cult site constrained by sediment and rock surface luminescence dating techniques. *Quat. Geochronol.* **30**, 90–99 (2015).
47. Gkinis, V. et al. A 120,000-year long climate record from a NW-Greenland deep ice core at ultra-high resolution. *Sci. Data* **8**, 141 (2021).
48. Nye, J. F. The distribution of stress and velocity in glaciers and ice-sheets. *Proc. R. Soc. London, Ser. A.* **239**, 113–133 (1957).
49. Rieckh, T., Born, A., Robinson, A., Law, R. & Gülle, G. Design and performance of ELSA v2.0: an isochronal model for ice-sheet layer tracing. *Geosci. Model Dev.* **17**, 6987–7000 (2024).

50. Born, A. & Robinson, A. Modeling the Greenland englacial stratigraphy. *Cryosphere* **15**, 4539–4556 (2021).
51. MacGregor, J. A. et al. Holocene deceleration of the Greenland Ice Sheet. *Science* **351**, 590–593 (2016).
52. MacGregor, J. A. et al. A synthesis of the basal thermal state of the Greenland Ice Sheet. *J. Geophys. Res. F: Earth Surf.* **121**, 1328–1350 (2016).
53. Walcott-George, C. K. et al. Luminescence dating results from the 2023 ASIG sediment core, Prudhoe Dome, Greenland. *Zenodo* https://doi.org/10.5281/zenodo.17047557 (2025).
54. Gkinis, V. et al. Stable water isotopes ($\delta^{17}O$, $\delta^{18}O$, δD) from deep ice at Prudhoe Dome, NW Greenland. *Pangaea* https://doi.org/10.1594/PANGAEA.984743 (2025).
55. Walcott-George, C. K. et al. Ice depth-age models for Prudhoe Dome, Greenland. *Zenodo* https://doi.org/10.5281/zenodo.17048034 (2025).

Acknowledgements

We thank the people and government of Kalaallit Nunaat (Greenland) for allowing us to conduct research on the island. Thank you to R. Erickson, F. R. Harmon and the National Science Foundation Ice Drilling Program for drill operations; J. Þorbjörnsson and T. Nave for field support; Polar Field Services, especially K. Cosper, for field logistics; Kenn Borek Air, Air Greenland and M. Vogt at Volcano Heli for flights; and Pituffik Space Base for pre- and post-field support. NSF grants 1933938 (J.P.B.), 1933927 (J.M.S., N.E.Y.), 1934477 (R.M.D.), 1933802 (S.A.) supported this research. V.G. acknowledges funding from the Danish Research Foundation (grant 'Iso-DeepIce' 10.46540/2032-00228B). J.M.S. acknowledges support from the Vetlesen Foundation.

Author contributions

C.K.W.-G., N.D.B. and J.P.B. designed the study. C.K.W.-G., J.P.B., A.B.-K., N.E.Y., T.K., E.R.M., S.A., N.T.S. and J.M.S. conducted fieldwork. C.K.W.-G., N.D.B., A.B.-K. and V.G. conducted sample preparation and lab analyses. J.A.M. modelled the age of the basal ice. C.K.W.-G., N.D.B. and J.P.B. conducted initial data analysis and interpretation, with input from all authors. C.K.W.-G., N.D.B. and J.P.B. drafted all figures and wrote the first draft of the manuscript. All authors contributed substantially to additional iterations. J.P.B., N.E.Y., S.A., R.D. and J.M.S. acquired funding.

Competing interests

The authors declare no competing interests.

Additional information

Extended data is available for this paper at https://doi.org/10.1038/s41561-025-01889-9.

Supplementary information The online version contains supplementary material available at https://doi.org/10.1038/s41561-025-01889-9.

Correspondence and requests for materials should be addressed to Caleb K. Walcott-George.

Peer review information *Nature Geoscience* thanks José Fernández-Fernández, Jerry Lloyd and Marion McKenzie for their contribution to the peer review of this work. Primary Handling Editor: James Super, in collaboration with the *Nature Geoscience* team.

https://doi.org/10.1038/s41561-025-01889-9

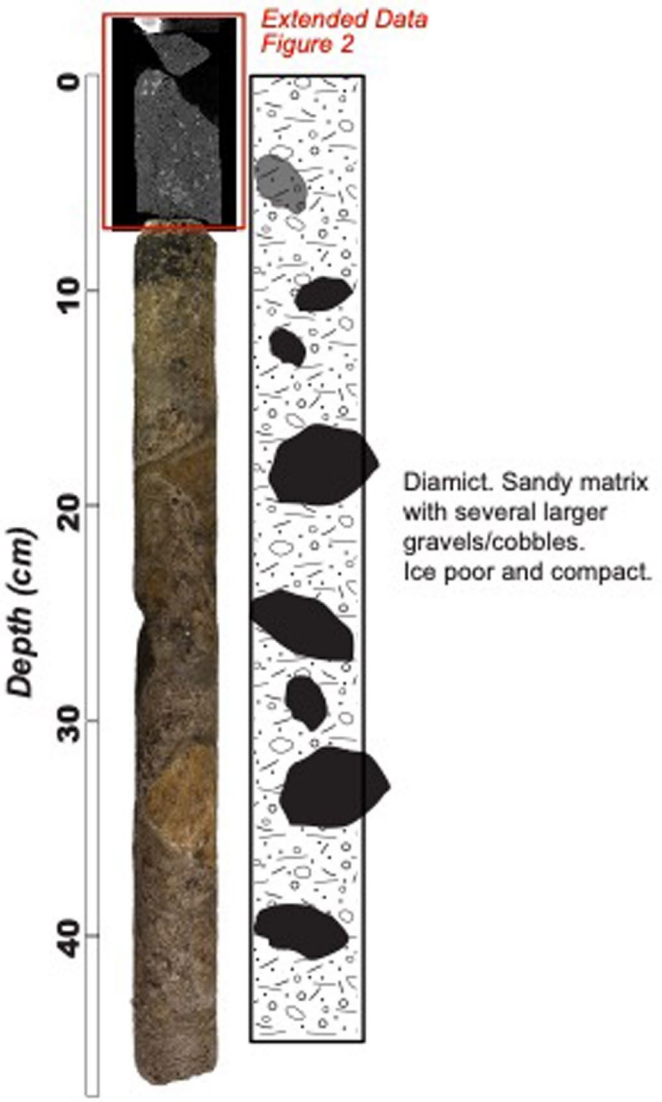

Extended Data Fig. 1 | ASIG Core log and core images/CT scans. CT scan is shown for the uppermost 7.5 cm collected in the dark. Photos are from the lower sections.

https://doi.org/10.1038/s41561-025-01889-9

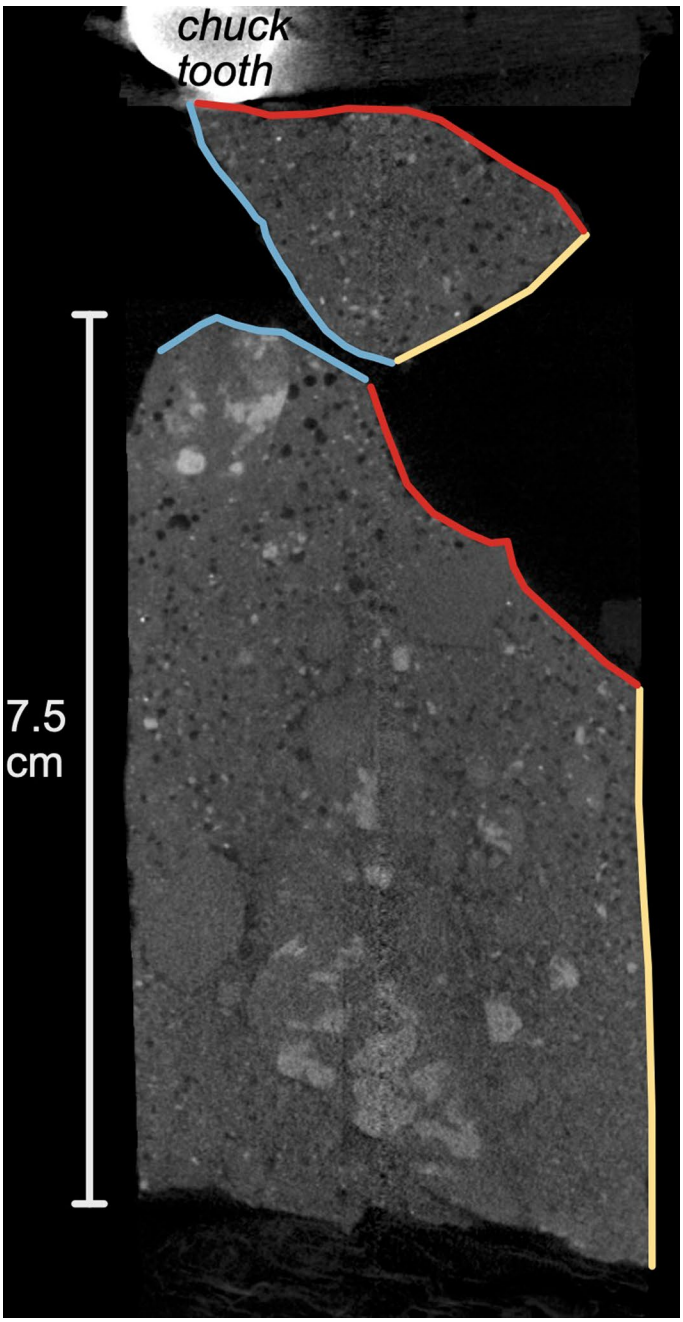

Extended Data Fig. 2 | CT scan image of the uppermost 7.5 cm of sediment from the ASIG core. Sediment was collected in an opaque PVC tube for luminescence analysis. During drilling or sample extraction, a chunk of the uppermost sediment became loose. However, using the CT scan image, we were able to reconstruct its original orientation. In this image, the red lines on both chunks show where they were connected, the blue line shows the original top surface, and the yellow line shows the original side surface. The bright spot in the top of the image is a tooth from the drill chuck that was dropped down the borehole during drill operations.

https://doi.org/10.1038/s41561-025-01889-9

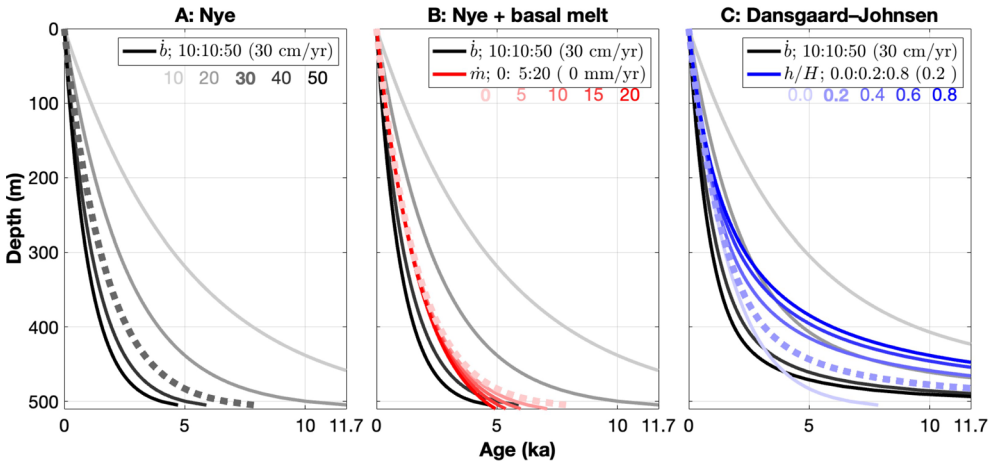

Extended Data Fig. 3 | One-dimensional steady-state models of the depth–age relationship of the ice column at the Prudhoe drill site. For each model parameter in each model/panel, a range of five values is considered (see legend), and the resulting depth-age relationship shown is darker for increasing values. For each model/panel, the best estimate of the modern value is shown as a thicker dashed line. A): Nye (sandwich) model depends only on accumulation rate (bdot), the ice column deforms uniformly by pure shear and is not melting at the bed. B): Nye+melt model is the same as Nye (A), except that basal melting (mdot) is included. C): Dansgaard-Johnsen model, where the ice column of thickness H deforms by pure shear above a height h above the bed, and by simple shear below it. The first two models (Nye and Nye+melt) tend to produce younger ice columns, and regardless of parameter selection, they consistently indicate a completely Holocene ice column. The latter model (Dansgaard–Johnsen) indicates that a non-negligible basal layer of Pleistocene ice is possible at lower accumulation rates and higher basal shear layer thicknesses. From this initial modeling, we conclude that no past major basal shear or melting is required to reproduce the measured the $\delta^{18}O$ drill ice chip record, and that simplest explanation for that record is an ice cap that regrew under a mean ice accumulation rate slightly lower than present.